**SANDIA REPORT**
SAND2000–8201
Unlimited Release
Printed January 2000

# Pulsating Hydrodynamic Instability and Thermal Coupling in an Extended Landau/Levich Model of Liquid-Propellant Combustion ---II. Viscous Analysis

Stephen B. Margolis

Prepared by
Sandia National Laboratories
Albuquerque, New Mexico 87185 and Livermore, California 94550

Sandia is a multiprogram laboratory operated by Sandia Corporation, a Lockheed Martin Company, for the United States Department of Energy under Contract DE-AC04-94AL85000.





Sandia National Laboratories

Issued by Sandia National Laboratories, operated for the United States Department of Energy by Sandia Corporation.



Available to DOE and DOE contractors from
Office of Scientific and Technical Information
P.O. Box 62
Oak Ridge, TN 37831

Prices available from (703) 605-6000
Web site: http://www.ntis.gov/ordering.htm

Available to the public from
National Technical Information Service
U.S. Department of Commerce
5285 Port Royal Rd
Springfield, VA 22161

NTIS price codes
Printed copy: A03
Microfiche copy: A01

## DISCLAIMER

Portions of this document may be illegible in electronic image products. Images are produced from the best available original document.

SAND2000-8201
Unlimited Release
Printed January 2000

# PULSATING HYDRODYNAMIC INSTABILITY AND THERMAL COUPLING IN AN EXTENDED LANDAU/LEVICH MODEL OF LIQUID-PROPELLANT COMBUSTION — II. VISCOUS ANALYSIS

STEPHEN B. MARGOLIS*†
Sandia National Laboratories, Livermore, California 94551-0969

## Abstract

A pulsating form of hydrodynamic instability has recently been shown to arise during liquid-propellant deflagration in those parameter regimes where the pressure-dependent burning rate is characterized by a negative pressure sensitivity. This type of instability can coexist with the classical cellular, or Landau, form of hydrodynamic instability, with the occurrence of either dependent on whether the pressure sensitivity is sufficiently large or small in magnitude. For the inviscid problem, it has been shown that when the burning rate is realistically allowed to depend on temperature as well as pressure, that sufficiently large values of the temperature sensitivity relative to the pressure sensitivity causes the pulsating form of hydrodynamic instability to become dominant. In that regime, steady, planar burning becomes intrinsically unstable to pulsating disturbances whose wavenumbers are sufficiently small. In the present work, this analysis is extended to the fully viscous case, where it is shown that although viscosity is stabilizing for intermediate and larger wavenumber perturbations, the intrinsic pulsating instability for small wavenumbers remains. Under these conditions, liquid-propellant combustion is predicted to be characterized by large unsteady cells along the liquid/gas interface.

*Principal Member of Technical Staff, Combustion Research Facility/MS 9052/margoli@sandia.gov.

†This work was supported by the U.S. Department of Energy under contract DE-AC04-94AL85000 and by the NASA Microgravity Science Research Program under contract C-32031-E.

# PULSATING HYDRODYNAMIC INSTABILITY AND THERMAL COUPLING IN AN EXTENDED LANDAU/LEVICH MODEL OF LIQUID-PROPELLANT COMBUSTION — II. VISCOUS ANALYSIS

## Introduction

Hydrodynamic (Landau) instability in combustion is typically associated with the onset of wrinkling of a flame surface, corresponding to the formation of steady cellular structures as the stability threshold is crossed. This type of instability was originally described by Landau [1], and is attributed to thermal expansion across a combustion front. Although gaseous combustion was determined to be intrinsically unstable in Landau's analysis, it was demonstrated that additional effects, such as gravity and surface tension, that enter when the unburned mixture is a liquid result in a specific stability criterion. However, this analysis, along with a later study by Levich [2] that considered viscous effects in lieu of surface tension, assumed that the the combustion front propagated normal to itself with constant speed, whereas it is now recognized that there is a dynamic interaction between the burning rate and local conditions at the front.

For those problems in which pyrolysis, exothermic decomposition and/or combustion occurs in an intrusive region in the vicinity of the liquid/gas interface, the dynamical coupling of the burning rate with the underlying hydrodynamics of the flow can be achieved through an analysis of the thin combustion/interface region. An alternative approach, however, is to simply postulate a phenomenological dependence of the local burning rate on pressure and temperature, and to obtain results in terms of suitably defined sensitivity parameters. Both types of methodologies have been applied to the problem of solid-propellant combustion, and each offers certain advantages [3,4]. In the present series of studies on liquid-propellant combustion [5–7], the latter approach has been adopted, thereby generalizing the Landau/Levich model to allow for a coupling of the burning rate with the local pressure and temperature fields.

Summarizing some of the results obtained from the present model, it has been shown that when only the pressure sensitivity of the burning rate is taken into account, an appropriately generalized stability criterion for cellular (Landau) instability is obtained. Exploiting the realistic limit of small gas-to-liquid density ratios, it is found that the stable region occurs for negative

values of the pressure-sensitivity parameter, with the original Landau model being intrinsically unstable in this limit. In particular, the neutral stability boundary possesses a local minimum when plotted against the disturbance wavenumber, suggesting that as the pressure-sensitivity parameter decreases in magnitude, the liquid/gas interface/front develops cells corresponding to classical hydrodynamic instability [5]. This minimum reflects the fact that surface tension and viscosity are stabilizing influences for short-wave disturbances, whereas gravity is a stabilizing influence for long-wave perturbations. As a result, the effect of reducing the gravitational acceleration to microgravity levels is to shift the neutral stability minimum to smaller wavenumbers. Thus, in the microgravity regime, Landau instability becomes a long-wave instability phenomenon, implying the appearance of large cells along the combustion interface.

Aside from the classical cellular form of hydrodynamic instability, this dynamic generalization of the Landau/Levich model also predicts the appearance of a *pulsating* form of hydrodynamic instability, corresponding to the onset of temporal oscillations in the location of the liquid/gas interface. This form of hydrodynamic instability occurs for negative values of the pressure-sensitivity parameter that are sufficiently large in magnitude [6]. Consequently, stable, planar burning is predicted to occur in a range of negative pressure sensitivities that lies below the cellular boundary and above the pulsating boundary just described. A stable range of negative pressure sensitivities is applicable, for example, to certain types of hydroxylammonium nitrate (HAN)-based liquid propellants at low pressures for which nonsteady modes of combustion have been observed [8]. The appearance of both pulsating and cellular forms of hydrodynamic instability is analogous to the two corresponding types of thermal/diffusive instabilities that occur for sufficiently large and sufficiently small Lewis numbers, respectively [9].

When the effect of a temperature sensitivity in the burning rate is included in the analysis, substantial modifications to the above stability description can occur. Specifically, if the temperature-sensitivity parameter is sufficiently large relative to the parameter corresponding to pressure sensitivity, the pulsating hydrodynamic stability boundary can develop a turning point (*i.e.*, become C-shaped) in the (disturbance-wavenumber, pressure-sensitivity) plane. In that case, the stable region for small wavenumbers disappears, and liquid-propellant combustion is predicted to be intrinsically unstable to the nonsteady form of hydrodynamic instability for all sufficiently

large disturbance wavelengths. This has been described in detail in the limit of zero viscosity [7], and the purpose of the present work is to extend that analysis to the fully viscous model. Viscous effects were shown to have a substantial influence in the absence of thermal sensitivity, where it turned out that the stable region became significantly widened when viscosity was present, and the same result will be demonstrated when thermal effects are present. However, the same intrinsic pulsating instability that occurs for sufficiently large temperature sensitivities and sufficiently small wavenumbers in the inviscid case will be shown to be preserved even when viscosity is included. These results lend further support to the notion that a likely form of hydrodynamic instability in liquid-propellant combustion is of a nonsteady, long-wave nature, distinct from the steady, cellular form originally predicted by Landau.

## Summary of the Mathematical Model

The mathematical model was described previously [5,10], but is briefly summarized here for completeness. Specifically, it is assumed that the combustion front coincides with the liquid/gas interface, where pyrolysis and/or exothermic decomposition occurs. Denoting the nondimensional location of this downward-propagating interface by $x_3 = \Phi(x_1, x_2, t)$, where $x_3$ is the vertical coordinate and the adopted coordinate system is fixed with respect to the stationary liquid at $x_3 = -\infty$, we transform to the moving coordinate system $x = x_1$, $y = x_2$, $z = x_3 - \Phi(x_1, x_2, t)$ such that the liquid/gas interface always lies at $z = 0$. Conservation of mass, energy and momentum within each phase then gives

$$\nabla \cdot \mathbf{v} = 0\,, \quad z \neq 0\,, \tag{1}$$

$$\frac{\partial \Theta}{\partial t} - \frac{\partial \Phi}{\partial t}\frac{\partial \Theta}{\partial z} + \mathbf{v} \cdot \nabla \Theta = \left\{ \begin{matrix} 1 \\ \lambda \end{matrix} \right\} \nabla^2 \Theta\,, \quad z \lesseqgtr 0\,, \tag{2}$$

$$\frac{\partial \mathbf{v}}{\partial t} - \frac{\partial \Phi}{\partial t}\frac{\partial \mathbf{v}}{\partial z} + (\mathbf{v} \cdot \nabla)\mathbf{v} = (0, 0, -Fr^{-1}) - \left\{ \begin{matrix} 1 \\ \rho^{-1} \end{matrix} \right\} \nabla p + \left\{ \begin{matrix} Pr_l \\ \lambda Pr_g \end{matrix} \right\} \nabla^2 \mathbf{v}\,, \quad z \lesseqgtr 0\,, \tag{3}$$

where $\mathbf{v}$, $\Theta$ and $p$ denote velocity, temperature and pressure, respectively, $Pr_l$ and $Pr_g$ denote the liquid and gas-phase Prandtl numbers, $\rho$, $\lambda$ and $c$ (used below) are the gas-to-liquid density, thermal diffusivity and heat-capacity ratios, and $Fr^{-1}$ is the inverse Froude number (gravitational acceleration). Other nondimensional parameters introduced below include the liquid surface-tension coefficient $\gamma$, the gas-to-liquid viscosity ratio $\mu$ ($\rho\lambda Pr_g = \mu Pr_l$), the rate-of-strain tensor $\mathbf{e}$ and

the unburned-to-burned temperature ratio $\sigma_u$.

Equations (1) - (3) are subject to a set of boundary and interface conditions given by

$$\mathbf{v} = \mathbf{0}\,,\ \Theta = 0 \text{ at } z = -\infty\,, \quad \Theta = 1 \text{ at } z = +\infty\,, \quad \Theta|_{z=0^-} = \Theta|_{z=0^+}\,, \tag{4}$$

$$\hat{\mathbf{n}}_s \times \mathbf{v}_- = \hat{\mathbf{n}}_s \times \mathbf{v}_+\,, \tag{5}$$

$$\hat{\mathbf{n}}_s{\cdot}(\mathbf{v}_- - \rho\mathbf{v}_+) = (1-\rho)S(\Phi)\frac{\partial \Phi}{\partial t}\,, \tag{6}$$

$$\hat{\mathbf{n}}_s{\cdot}\mathbf{v}_- - S(\Phi)\frac{\partial \Phi}{\partial t} = A(p|_{z=0^+}, \Theta|_{z=0})\,, \tag{7}$$

$$\begin{aligned} p|_{z=0^-} - p|_{z=0^+} &= \hat{\mathbf{n}}_s{\cdot}\left[\rho\mathbf{v}_+(\hat{\mathbf{n}}_s\cdot\mathbf{v}_+) - \mathbf{v}_-(\hat{\mathbf{n}}_s\cdot\mathbf{v}_-) - \rho\lambda Pr_g \mathbf{e}_+\cdot\hat{\mathbf{n}}_s + Pr_l \mathbf{e}_-\cdot\hat{\mathbf{n}}_s\right] \\ &\quad + \hat{\mathbf{n}}_s{\cdot}(\mathbf{v}_- - \rho\mathbf{v}_+)S(\Phi)\frac{\partial \Phi}{\partial t} - \gamma(-\nabla\cdot\hat{\mathbf{n}}_s)\,, \end{aligned} \tag{8}$$

$$\hat{\mathbf{n}}_s{\times}\left[\rho\mathbf{v}_+(\hat{\mathbf{n}}_s\cdot\mathbf{v}_+) - \mathbf{v}_-(\hat{\mathbf{n}}_s\cdot\mathbf{v}_-) + (\mathbf{v}_- - \rho\mathbf{v}_+)S(\Phi)\frac{\partial \Phi}{\partial t}\right] = \hat{\mathbf{n}}_s{\times}(\rho\lambda Pr_g \mathbf{e}_+\cdot\hat{\mathbf{n}}_s - Pr_l \mathbf{e}_-\cdot\hat{\mathbf{n}}_s)\,, \tag{9}$$

$$\begin{aligned} \hat{\mathbf{n}}_s\cdot(c\rho\lambda\nabla\Theta|_{z=0^+} - \nabla\Theta|_{z=0^-}) &= \hat{\mathbf{n}}_s{\cdot}\left[(c\rho\mathbf{v}_+ - \mathbf{v}_-)\Theta|_{z=0} + \hat{c}(\sigma_u\rho\mathbf{v}_+ - \mathbf{v}_-)\right] \\ &\quad + \left[(1-c\rho)\Theta|_{z=0} + \hat{c}(1-\sigma_u\rho)\right]S(\Phi)\frac{\partial \Phi}{\partial t}\,, \quad \hat{c} = c/(1-\sigma_u)\,, \end{aligned} \tag{10}$$

where $\mathbf{v}_\pm = \mathbf{v}|_{z=0^\pm}$, $\mathbf{e}_\pm = \mathbf{e}|_{z=0^\pm}$, and Eqs. (5) – (10) correspond to continuity of the transverse velocity components (no-slip), conservation of (normal) mass flux, the mass burning rate (pyrolysis) law, conservation of flux of the normal and transverse components of momentum, and conservation of heat flux. Here, $S(\Phi) = \left(1+\Phi_x^2+\Phi_y^2\right)^{-1/2}$, the unit normal $\hat{\mathbf{n}}_s = \left(-\Phi_x, -\Phi_y, 1\right)S(\Phi)$, and the expressions for the gradient operator, the Laplacian and the curvature in the moving coordinate system are given by $\nabla = \left(\partial_x - \Phi_x\partial_z, \partial_y - \Phi_y\partial_z, \partial_z\right)$, $\nabla^2 = \partial_{xx} + \partial_{yy} + \left(1+\Phi_x^2+\Phi_y^2\right)\partial_{zz} - 2\Phi_x\partial_{xz} - 2\Phi_y\partial_{yz} - \left(\Phi_{xx}+\Phi_{yy}\right)\partial_z$ and $-\nabla\cdot\hat{\mathbf{n}}_s = \Phi_{xx}\left(1+\Phi_y^2\right) + \Phi_{yy}\left(1+\Phi_x^2\right) - 2\Phi_x\Phi_y\Phi_{xy}\right)$, respectively. However, the vector $\mathbf{v}$ still denotes the velocity with respect to the $(x_1, x_2, x_3)$ coordinate system. Finally, we note that the nondimensional mass burning rate appearing in Eq. (7) is assumed to be functionally dependent on both the local pressure and temperature at the liquid/gas interface. By definition, $A = 1$ for the case of steady, planar burning, but perturbations in pressure and/or temperature result in corresponding perturbations in the local mass burning rate.

Since the thermal and hydrodynamic fields are coupled only through the temperature dependence of the mass burning rate $A$ appearing in Eq. (7), the strictly hydrodynamic problem for $p$, $\mathbf{v}$ and $\Phi_s$ can be analyzed separately when $A$ is assumed to depend on pressure only [5,6]. In the present work, we focus on the fully coupled problem to determine how the hydrodynamic

stability boundaries are modified when the local burning rate depends on temperature as well as pressure. Our stability results will thus depend on two sensitivity parameters, $A_p$ and $A_\Theta$, defined as $A_p = \partial A/\partial p|_{\Theta=1,p=0}$ and $A_\Theta = \partial A/\partial \Theta|_{\Theta=1,p=0}$, where $\Theta = 1$ and $p = 0$ denote the interface values of temperature and pressure of the basic solution in Eq. (11) below. Though an explicit expression for the reaction rate $A$ is not needed in the present analysis, we note that since the nondimensional activation energy is typically large, the temperature sensitivity $A_\Theta$ would likely be larger in magnitude than the pressure sensitivity $A_p$, a fact that will have some bearing on the relative scalings of these parameters that will emerge in the following analysis.

## The Basic Solution and its Linear Stability

The nontrivial basic solution of the above problem that corresponds to the special case of a steady, planar deflagration is given by

$$\begin{gathered}\Phi^0 = -t\,, \quad \mathbf{v}^0 = (0,0,v^0)\,, \quad v^0 = \begin{cases} 0, & z<0 \\ \rho^{-1}-1, & z>0\,, \end{cases} \\ \Theta^0(z) = \begin{cases} e^z, & z<0 \\ 1, & z>0\,, \end{cases} \quad p^0(z) = \begin{cases} -Fr^{-1}z + \rho^{-1} - 1, & z<0 \\ -\rho Fr^{-1} z, & z>0\,. \end{cases}\end{gathered} \tag{11}$$

The problem governing its linear stability may be formulated, prior to introducing any further approximations, in a standard fashion by introducing the perturbation quantities $\phi(x,y,t) = \Phi(x,y,z,t) - \Phi^0(t)$, $\mathbf{u}(x,y,z,t) = \mathbf{v}(x,y,z,t) - \mathbf{v}^0(z)$, $\zeta(x,y,z,t) = p(x,y,z,t) - p^0(z)$ and $\theta(x,y,z,t) = \Theta - \Theta^0(z) - \phi_s d\Theta^0/dz$. The problem obtained when Eqs. (1) – (10) are linearized about the basic solution (11) is then given in terms of these perturbation variables by

$$\frac{\partial u_1}{\partial x} + \frac{\partial u_2}{\partial y} + \frac{\partial u_3}{\partial z} = 0\,, \quad z \neq 0\,, \tag{12}$$

$$\begin{aligned}\left\{\begin{matrix}1\\ \rho\end{matrix}\right\}\frac{\partial \mathbf{u}}{\partial t} + \frac{\partial \mathbf{u}}{\partial z} = &-\left(\frac{\partial \zeta}{\partial x} + \left\{\begin{matrix}1\\ \rho\end{matrix}\right\}Fr^{-1}\frac{\partial \phi}{\partial x}, \frac{\partial \zeta}{\partial y} + \left\{\begin{matrix}1\\ \rho\end{matrix}\right\}Fr^{-1}\frac{\partial \phi}{\partial y}, \frac{\partial \zeta}{\partial z}\right) \\ &+ \left\{\begin{matrix}Pr_l\\ \mu Pr_l\end{matrix}\right\}\left(\frac{\partial^2 \mathbf{u}}{\partial x^2} + \frac{\partial^2 \mathbf{u}}{\partial y^2} + \frac{\partial^2 \mathbf{u}}{\partial z^2}\right), \quad z \lesseqgtr 0\,,\end{aligned} \tag{13}$$

$$\left\{\begin{matrix}1\\ \rho\end{matrix}\right\}\frac{\partial \theta}{\partial t} + \frac{\partial \theta}{\partial z} = \left\{\begin{matrix}-u_3\, e^z\\ 0\end{matrix}\right\} + \left\{\begin{matrix}1\\ \rho\lambda\end{matrix}\right\}\left(\frac{\partial^2 \theta}{\partial x^2} + \frac{\partial^2 \theta}{\partial y^2} + \frac{\partial^2 \theta}{\partial z^2}\right), \quad z \lesseqgtr 0\,, \tag{14}$$

$$\mathbf{u} = \mathbf{0}\,,\ \theta = 0 \text{ at } z = -\infty\,, \quad \theta = 0 \text{ at } z = +\infty\,, \quad \theta|_{z=0^+} - \theta|_{z=0^-} = \phi_s\,, \tag{15}$$

$$u_1\big|_{z=0^-} - u_1\big|_{z=0^+} = (\rho^{-1}-1)\phi_x\,, \quad u_2\big|_{z=0^-} - u_2\big|_{z=0^+} = (\rho^{-1}-1)\phi_y\,, \tag{16}$$

$$u_3\big|_{z=0^-} - \rho u_3\big|_{z=0^+} = (1-\rho)\phi_t\,, \quad u_3\big|_{z=0^-} - \phi_t = A_p\zeta|_{z=0^+} + A_\Theta\theta|_{z=0^+}\,, \tag{17}$$

$$\zeta|_{z=0^-} - \zeta|_{z=0^+} = 2\big(u_3\big|_{z=0^+} - u_3\big|_{z=0^-}\big) + 2Pr_l\Big(\frac{\partial u_3}{\partial z}\Big|_{z=0^-} - \mu\frac{\partial u_3}{\partial z}\Big|_{z=0^+}\Big) - 2(1-\rho)\phi_t - \gamma\left(\phi_{xx}+\phi_{yy}\right), \tag{18}$$

$$\mu Pr_l\Big(\frac{\partial u_1}{\partial z}\Big|_{z=0^+} + \frac{\partial u_3}{\partial x}\Big|_{z=0^+}\Big) - Pr_l\Big(\frac{\partial u_1}{\partial z}\Big|_{z=0^-} + \frac{\partial u_3}{\partial x}\Big|_{z=0^-}\Big) = 0\,, \tag{19}$$

$$\mu Pr_l\Big(\frac{\partial u_2}{\partial z}\Big|_{z=0^+} + \frac{\partial u_3}{\partial y}\Big|_{z=0^+}\Big) - Pr_l\Big(\frac{\partial u_2}{\partial z}\Big|_{z=0^-} + \frac{\partial u_3}{\partial y}\Big|_{z=0^-}\Big) = 0\,, \tag{20}$$

$$c\rho\lambda\frac{\partial\theta}{\partial z}\Big|_{z=0^+} - \frac{\partial\theta}{\partial z}\Big|_{z=0^-} - c\theta|_{z=0^+} + \theta|_{z=0^-} = -u_3\big|_{z=0^-} + \phi_t\,, \tag{21}$$

where Eqs. (16) and (17) have been used to simplify Eqs. (18) – (21).

Nontrivial harmonic solutions for $\phi$, $\mathbf{u}$ and $\zeta$, proportional to $e^{i\omega t+ik_1x+ik_2y}$, that satisfy Eqs. (12) - (14) and the boundary/boundedness conditions at $z=\pm\infty$ are given by $\phi = e^{i\omega t+ik_1x+ik_2y}$ and

$$\zeta = e^{i\omega t+ik_1x+ik_2y}\begin{cases} b_1e^{kz} - Fr^{-1}, & z<0 \\ b_2e^{-kz} - \rho Fr^{-1}, & z>0\,, \end{cases} \tag{22}$$

$$u_1 = e^{i\omega t+ik_1x+ik_2y}\begin{cases} b_3e^{qz} - ik_1(i\omega+k)^{-1}b_1e^{kz}, & z<0 \\ b_4e^{rz} - ik_1(i\omega\rho-k)^{-1}b_2e^{-kz}, & z>0\,, \end{cases} \tag{23}$$

$$u_2 = e^{i\omega t+ik_1x+ik_2y}\begin{cases} b_5e^{qz} - ik_2(i\omega+k)^{-1}b_1e^{kz}, & z<0 \\ b_6e^{rz} - ik_2(i\omega\rho-k)^{-1}b_2e^{-kz}, & z>0\,, \end{cases} \tag{24}$$

$$u_3 = e^{i\omega t+ik_1x+ik_2y}\begin{cases} b_7e^{qz} - k(i\omega+k)^{-1}b_1e^{kz}, & z<0 \\ b_8e^{rz} + k(i\omega\rho-k)^{-1}b_2e^{-kz}, & z>0\,, \end{cases} \tag{25}$$

$$\theta = e^{i\omega t+ik_1x+ik_2y}\begin{cases} b_9e^{pz} - [i\omega+k^2-q(q+1)]^{-1}b_7e^{(q+1)z} + k[(i\omega)^2-k^2]^{-1}b_1e^{(k+1)z}, & z<0 \\ b_{10}e^{sz}, & z>0\,. \end{cases} \tag{26}$$

Here, $k = \left(k_1^2+k_2^2\right)^{1/2}$ is the overall disturbance wavenumber and the quantities $p$, $q$, $r$, $s$ are defined as $2p = 1+\left[1+4(i\omega+k^2)\right]^{1/2}$, $2Pr_l\,q = 1+\left[1+4Pr_l(i\omega+Pr_l\,k^2)\right]^{1/2}$, $2\mu Pr_l\,r = 1-\left[1+4\mu Pr_l(i\omega\rho+\mu Pr_l\,k^2)\right]^{1/2}$ and $2\rho\lambda s = 1-\left[1+4\rho^2\lambda(i\omega+\lambda k^2)\right]^{1/2}$. Substituting this solution into the interface conditions (16) - (21) and using Eq. (12) for $z \lesseqgtr 0$ yields eleven conditions for the ten coefficients $b_1$ - $b_{10}$ and the complex frequency (dispersion relation) $i\omega(k)$. In particular, these conditions are given by

$$ik_1b_3 + ik_2b_5 + qb_7 = ik_1b_4 + ik_2b_6 + rb_8 = 0\,, \tag{27}$$

$$b_3 - \frac{ik_1}{i\omega+k}b_1 - b_4 + \frac{ik_1}{i\omega\rho-k}b_2 = (\rho^{-1}-1)ik_1\,, \quad b_5 - \frac{ik_2}{i\omega+k}b_1 - b_6 + \frac{ik_2}{i\omega\rho-k}b_2 = (\rho^{-1}-1)ik_2\,, \tag{28}$$

$$b_7 - \frac{k}{i\omega + k} b_1 - \rho b_8 - \frac{\rho k}{i\omega\rho - k} b_2 = (1-\rho) i\omega\,, \quad b_7 - \frac{k}{i\omega + k} b_1 - A_p\, b_2 - A_\Theta\, b_{10} = i\omega - \rho Fr^{-1} A_p\,, \tag{29}$$

$$\left[1 + \frac{2k^2 Pr_l}{i\omega + k}\right] b_1 - \left[1 + \frac{2k(k\mu Pr_l + 1 - \rho)}{i\omega\rho - k}\right] b_2 - 2Pr_l\, q b_7 - 2(1 - \rho - \mu Pr_l\, r) b_8 = (1-\rho)(Fr^{-1} - 2i\omega) + \gamma k^2\,, \tag{30}$$

$$\mu Pr_l\, r b_4 + \frac{2ik_1 k\mu Pr_l}{i\omega\rho - k} b_2 + ik_1 \mu Pr_l\, b_8 - Pr_l\, q b_3 + \frac{2ik_1 k Pr_l}{i\omega + k} b_1 - ik_1 Pr_l\, b_7 = 0\,, \tag{31}$$

$$\mu Pr_l\, r b_6 + \frac{2ik_2 k\mu Pr_l}{i\omega\rho - k} b_2 + ik_2 \mu Pr_l\, b_8 - Pr_l\, q b_5 + \frac{2ik_2 k Pr_l}{i\omega + k} b_1 - ik_2 Pr_l\, b_7 = 0\,, \tag{32}$$

$$b_{10} - b_9 + [i\omega + k^2 - q(q+1)]^{-1} b_7 - k[(i\omega)^2 - k^2]^{-1} b_1 = 1\,, \tag{33}$$

$$(1 - c + c\rho\lambda s) b_{10} - p b_9 + \left[\frac{q+1}{i\omega + k^2 - q(q+1)} + 1\right] b_7 - \frac{k}{i\omega + k}\left[\frac{k+1}{i\omega - k} + 1\right] b_1 = 1 + i\omega\,. \tag{34}$$

While the above problem is linear in the coefficients $b_1 - b_{10}$, which can thus be eliminated to give a single equation for $i\omega$, the resulting dispersion relation is quite long and highly nonlinear. Explicit results may be obtained for certain special cases, including the original problems considered by Landau [1] ($A_p = A_\Theta = Pr_l = \mu = 0$) and Levich [2] ($A_p = A_\Theta = \mu = \gamma = 0$), as well as a particular case ($A_\Theta = \mu = Pr_l = 0$) of the generalized model described above [5,11]. To obtain more general results, it is possible to exploit the smallness of certain parameters and to seek asymptotic solutions for the neutral stability boundaries. In particular, realistic limits to exploit include the smallness of the gas-to-liquid density and viscosity ratios $\rho$ and $\mu$, and, in the microgravity regime, $Fr^{-1}$. Pursuing this approach, tractable asymptotic results have so far been obtained for $A_\Theta = 0$ [5,6] and for the inviscid problem when $A_\Theta$ is nonzero [7]. The present work essentially completes the asymptotic analysis of the dispersion relation embodied in Eqs. (27) – (34) by extending the last of these studies to the fully viscous case.

### Parameter Scalings and Asymptotic Analysis of the Dispersion Relation

Focusing on the realistic regime $\rho \ll 1$ (typical values are on the order of $10^{-3}$ or $10^{-4}$), we formally introduce a bookkeeping parameter $\epsilon \ll 1$ and introduce the reasonable scalings $\rho = \rho^*\epsilon$, $\mu = \mu^*\epsilon$, $Pr_l \sim \mathrm{O}(1)$ and either $Fr^{-1} = g$ or $Fr^{-1} = g^*\epsilon$, where $Fr^{-1} \sim \mathrm{O}(\epsilon)$ corresponds to the case of greatly reduced gravity. In this parameter regime, the appropriate scaling for $A_p$ to describe the neutral stability region is $A_p = A_p^*\epsilon$ [5,6], whereas the appropriate scale that describes the main effects of thermal coupling turns out to be $A_\Theta = A_\Theta^*\epsilon^{1/4}$ [7]. Based on this scaling, we

note that the ratio $A_\Theta/A_p \sim O(\epsilon^{-3/4}) \gg 1$, as might be expected based on an overall Arrhenius reaction-rate dependence on temperature.

Based on our previous analyses, the scalings introduced above induce a set of corresponding regimes for the wavenumber $k$ (and the complex frequency $i\omega$) in the dispersion relation determined by Eqs. (27) – (34). These first emerged in our analysis of cellular instability using the generalized model in the limit $A_\Theta = 0$, but they are also relevant when one considers the pulsating form of instability and when $A_\Theta$ is allowed to be nonzero.In particular, in the case of cellular instability and zero temperature sensitivity, there are three wavenumber scales to be considered. First, there is an O(1) outer wavenumber region where the stabilizing effects of surface tension, viscosity and gravity are all relatively weak. Second, there is a far outer scale $k \sim k_f/\epsilon$ where surface tension and/or viscosity are strongly stabilizing and gravitational effects are, to a first approximation, negligible. Finally, we have an inner scale $k \sim k_i\epsilon$ or $k \sim k_i\epsilon^2$ where gravity is the dominant stabilizing effect (the first scale is valid for normal gravity, the latter for the reduced gravity regime), and where viscosity and surface-tension effects are absent at leading order. In each of these regimes, the cellular stability boundary, obtained by seeking solutions of the dispersion relation for which $i\omega$ is identically zero, is given respectively by

$$A_p^*(k) \sim -\rho^*/2\,, \qquad A_p^{*(i)}(k_i) \sim \begin{cases} \rho^*(\rho^* g - k_i)/2k_i, & Fr^{-1} \sim O(1) \\ \rho^*(\rho^* g^* - k_i)/2k_i, & Fr^{-1} \sim O(\epsilon)\,, \end{cases} \tag{35}$$

$$A_p^{*(f)} \sim -\rho^* + \frac{2\rho^*\mu^* P\left[1 + k_f(\rho^*\gamma + 2\mu^* P + 2\rho^* P)\right]}{4\mu^* P(1+\rho^* P k_f) - (1-R)(\rho^*\gamma + 2\mu^* P)}\,, \quad R = \left(1 + 4\mu^{*2} P^2 k_f^2\right)^{1/2}\,, \tag{36}$$

where $P \equiv Pr_l$. Matching these solutions to one another then leads to the composite stability boundary

$$A_p^{*(c)} \sim -\rho^* + \frac{2\rho^*\mu^* P\left[1 + \epsilon k(\rho^*\gamma + 2\mu^* P + 2\rho^* P)\right]}{4\mu^* P(1+\epsilon k\rho^* P) - (\rho^*\gamma + 2\mu^* P)\left[1 - (1 + 4\mu^{*2} P^2 \epsilon^2 k^2)^{1/2}\right]} + \frac{\rho^{*2}}{2k}\begin{cases} \epsilon g \\ \epsilon^2 g^*\,, \end{cases} \tag{37}$$

as shown in Fig. 1. Clearly, the stable region lies below $A_p^* = -\rho^*/2$ (negative values of $A_p$ over certain pressure ranges are characteristic of a number of HAN-based liquid propellants [8], with the location of the minimum in the cellular boundary increasing to less negative values of $A_p$ with increasing values of the stabilizing parameters $\gamma^*$, $Pr_l$, $\mu^*$ and $g$ (or $g^*$). Comparing the two sets of curves corresponding to the normal and reduced gravity cases, it is clear that the critical wavenumber for instability becomes small in the latter regime. That is, cellular hydrodynamic

instability becomes a long-wave instability in the limit of small gravitational acceleration. Further discussion of this stability boundary, and its relationship to the original Landau/Levich predictions, is given in [5].

Considering the pulsating stability boundary (in the limit $A_\Theta = 0$), which is obtained by seeking solutions of the dispersion relation for which only the real part of $i\omega$ vanishes, it is found [6] that the corresponding expressions in the inner and outer wavenumber regions are given by

$$A_p^* \sim -\rho^*\,, \qquad A_p^* \sim -\rho^*(1+2Pk)^{1/2}\,, \tag{38}$$

respectively. In this case, it is clear that the outer solution is, in fact, the composite solution, which lies below the cellular boundaries and recedes to negative values of $A_p$ that are larger in magnitude than $O(\epsilon)$ as $k$ becomes large (Fig. 2). Clearly, this stability boundary is more sensitive to the stabilizing effects of the liquid viscosity parameter $P$ than is the cellular boundary, having a leading-order stabilizing effect for O(1) wavenumber disturbances in this case. In the limit $P \to 0$, the pulsating boundary collapses to the straight line $A_p^* = -\rho^*$ (*i.e.*, $A_p^* = -1$ in Figs. 1 and 2), but even in that limit, there is a region of stability corresponding to values of $A_p^*$ greater than $-\rho^*$ and less than the minimum in the cellular boundary, which is greater than $-\rho^*/2$. However, if one now considers the effects of a nonzero temperature sensitivity in the inviscid limit $P = 0$, then, for $A_\Theta \sim O(\epsilon^{1/4})$, the pulsating boundary possesses a turning point such that the stability region disappears for sufficiently small wavenumber perturbations [7]. This is illustrated in Fig. 3, which indicates that the pulsating boundary then frames the stable region except along the upper branch that asymptotes to the previous cellular boundary as $k$ becomes large in the outer wavenumber region. The evolution from a stability diagram that indicates a stable region delineated by distinct pulsating and cellular hydrodynamic stability boundaries to the pulsating-dominated one shown in Fig. 3 can be shown to occur in the parameter regime $A_\Theta \sim O(\epsilon^{1/2})$, which, based on the estimate $A_\Theta/A_p \sim O\epsilon^{-1/2} \gtrsim 30$ (*i.e.*, of the same order as a typical nondimensional activation energy), appears to be attainable for many types of liquid propellants. We now extend the analysis that produced the fully-developed pulsating boundary shown in Fig. 3 to the viscous case in which both $P$ and $\mu^*$ are allowed to be nonzero.

Owing to the complexity of the fully viscous problem, we analyze Eqs. (27) – (34) directly by seeking appropriate expansions for the complex frequency $i\omega$ and the coefficients $b_i$. This differs

from our approach in the inviscid limit where it was feasible to first eliminate the $b_i$ in order to obtain a single implicit equation for $i\omega$ alone. We first consider the O(1) wavenumber region and, based on our previous analyses, seek an expansion for the dispersion relation $i\omega(k)$ in this region in the form

$$i\omega \sim \epsilon^{-1/2}(i\omega_0 + \epsilon^{1/4} i\omega_1 + \epsilon^{1/2} i\omega_2 + \cdots)\,, \tag{39}$$

Introducing the previously defined parameter scalings, the quantities $p$, $q$, $r$ and $s$ defined below Eq. (26) are expanded as

$$\begin{aligned} &p \sim p_{(-1/4)}\epsilon^{-1/4} + p_0 + p_{(1/4)}\epsilon^{1/4} + \cdots\,, \quad q \sim q_{(-1/4)}\epsilon^{-1/4} + q_0 + \cdots\,, \\ &r \sim r_{(1/2)}\epsilon^{1/2} + r_{3/4}\epsilon + r_1\epsilon + \cdots\,, \quad s \sim s_{(1/2)}(\epsilon^{1/2}) + \cdots\,, \end{aligned} \tag{40}$$

where $p_{(-1/4)} = (i\omega_0)^{1/2}$, $2p_0 = \left[1 + i\omega_1/(i\omega_0)^{1/2}\right]$, $8p_{(1/4)} = (i\omega_0)^{-1/2}\left[1 + 4k^2 + 4i\omega_2 - (i\omega_1)^2/i\omega_0\right]$, $q_{(-1/4)} = (i\omega_0/P)^{1/2}$, $2Pq_0 = \left[1 + i\omega_1/(i\omega_0/P)^{1/2}\right]$, $r_{(1/2)} = s_{(1/2)} = -i\omega_0\rho^*$, $r_{(3/4)} = -i\omega_1\rho^*$, and $r_1 = -i\omega_2\rho^* - (\mu^* Pk)^2$. Finally, the $b_i$ are conservatively postulated to have the expansions

$$\begin{aligned} b_i &= b_i^{(-1)}\epsilon^{-1} + b_i^{(-3/4)}\epsilon^{-3/4} + b_i^{(-1/2)}\epsilon^{-1/2} + \cdots\,, \quad i = 1,\, 2,\, 8\,, \\ b_i &= b_i^{(-1/2)}\epsilon^{-1/2} + b_i^{(-1/4)}\epsilon^{-1/4} + b_i^{(0)} + \cdots\,, \quad i = 3,\, 4,\, 5,\, 6\,, \\ b_i &= b_i^{(-1/4)}\epsilon^{-1/4} + b_i^{(0)}\epsilon^0 + b_i^{(1/4)}\epsilon^{1/4} + \cdots\,, \quad i = 7,\, 9,\, 10\,, \end{aligned} \tag{41}$$

where the form of the latter expansions is again partly motivated by our previous analyses of more specialized cases.

Substituting the above expansions into Eqs. (27) – (34) and equating coefficients of like powers of $\epsilon$, we obtain the leading-order conditions

$$ik_1 b_3^{(-1/2)} + ik_2 b_5^{(-1/2)} + q_{(-1/4)} b_7^{(-1/4)} = ik_1 b_4^{(-1/2)} + ik_2 b_6^{(-1/2)} + r_{(1/2)} b_8^{(-1)} = 0\,, \tag{42}$$

$$b_2^{(-1)} = -k^*/\rho^*\,, \quad b_1^{(-1)} = -(i\omega_0)^2/k\,, \quad b_9^{(-1/4)} = b_{10}^{(-1/4)} = 0\,, \tag{43}$$

$$b_1^{(-1)} + b_2^{(-1)} - 2b_8^{(-1)} = 0\,, \quad b_8^{(-1)} = -(k/\rho^*)(1 + A_p^*/\rho^*)\,, \tag{44}$$

where the last of these was obtained from the leading-order difference of the first and second of Eqs. (29) using the last of Eqs. (43). From Eqs. (43) and (44) we thus conclude that the leading-order dispersion relation is given by

$$(i\omega_0)^2 = (k/\rho^*)^2(2A_p^* + \rho^*)\,, \tag{45}$$

which is the same result as that obtained in the inviscid case when $A^*_\Theta = 0$. In particular, Eq. (45) implies that $(i\omega_0)^2 \gtrless 0$ for $A^*_p \gtrless -\rho^*/2$, which recovers the leading-order cellular boundary (35) for O(1) wavenumbers, but gives no definitive information regarding stability for $A^*_p < -\rho^*/2$ because $i\omega_0$ is purely imaginary in that region. That is, the stability of the basic solution in the latter region is determined by the real parts of higher-order coefficients in the expansion (39) for $i\omega$, although the fact that $\mathcal{I}m\{i\omega_0\} \neq 0$ implies that disturbances have a pulsating character for values of $A^*_p$ below the cellular stability boundary.

At the next order in the analysis of Eqs. (27) – (34), we obtain a second set of conditions given by

$$ik_1\, b_3^{(-1/4)} + ik_2\, b_5^{(-1/4)} + q_{(-1/4)}\, b_7^{(0)} + q_0\, b_7^{(-1/4)} = 0\,, \tag{46}$$

$$ik_1\, b_4^{(-1/4)} + ik_2\, b_6^{(-1/4)} + r_{(1/2)}\, b_8^{(-3/4)} + r_{(3/4)}\, b_8^{(-1)} = 0\,, \tag{47}$$

$$i\omega_1 = b_1^{(-3/4)} = b_2^{(-3/4)} = b_3^{(-1/2)} = b_5^{(-1/2)} = b_7^{(-1/4)} = b_9^{(0)} = b_{10}^{(0)} = b_8^{(-3/4)} = 0\,, \tag{48}$$

where the last of Eqs. (48) was deduced from the next-order difference of Eqs. (29). Finally, from the sum of the first of Eqs. (28) multiplied by $ik_1$ and the second of Eqs. (28) multiplied by $ik_2$, we conclude that $b_2^{(-1/2)} = i\omega_0(1 - A^*_p/\rho^*)$. However, the fact that $i\omega_1 = 0$ implies the need to continue the analysis at the next order to determine $i\omega_2$. Proceeding in this fashion, we obtain from the previous results and Eqs. (29) – (34) at this next higher order a new set of conditions given by

$$b_7^{(0)} - (k/i\omega_0) b_1^{(-1/2)} - 2i\omega_2 = k(1 - A^*_p/\rho^*)\,, \quad b_7^{(0)} = 0\,, \tag{49}$$

$$b_1^{(-1/2)} - 2b_8^{(-1/2)} = i\omega_0(2kP - 1 + A^*_p/\rho^*)\,, \tag{50}$$

$$b_8^{(-1/2)} - (A^*_\Theta/\rho^*) b_{10}^{(1/4)} = i\omega_0 \left[1 - (A^*_p/\rho^*)^2\right]\,, \tag{51}$$

$$-(k/i\omega_0) b_1^{(-1/2)} - (i\omega_0)^{1/2} b_{10}^{(1/4)} - 2i\omega_2 = 2Pk^2\,, \quad b_9^{(1/4)} = b_{10}^{(1/4)}\,, \tag{52}$$

where Eq. (51) was actually obtained from the next higher order difference of Eqs. (29), and the second of Eqs. (49) was obtained from the sum of Eqs. (31) multiplied by $ik_1$ and Eqs. (32) multiplied by $ik_2$. Equations (49) – (52) constitute a closed system for $b_1^{(-1/2)}$, $b_8^{(-1/2)}$, $b_{10}^{(1/4)}$ and $i\omega_2$. Eliminating the first three of these in favor of the last and using the result (45) for $i\omega_0$, the dispersion relation for $i\omega_2$ is finally obtained as

$$i\omega_2 = -2Pk^2 + k(A^*_p/\rho^* - 1)\left[A^*_p/\rho^* + 1 + \rho^{*-1/4} k^{-1/2} A^*_\Theta \left(2A^*_p/\rho^* + 1\right)^{-3/4}\right]. \tag{53}$$

Stability in the region $A_p^* < -\rho^*/2$ below the cellular boundary is determined by the real part of $i\omega_2$. In that region, the principal value of the complex factor in Eq. (53) may be written as $(A_p^*/\rho^*+1)^{-3/4} = \left[-(A_p^*/\rho^*+1)\right]^{-3/4} e^{-3i\pi/4}$, and thus the neutral stability condition $\mathcal{R}e\{i\omega_2\} = 0$ leads to an implicit equation for the (pulsating) neutral stability boundary $A_p^*(k; A_\Theta^*, P)$. In terms of the new pressure sensitivity parameter $\hat{b}$ defined by $A_p^* = -(\rho^*/2)(1+\hat{b})$, where $\hat{b}$ represents the negative deviation, in units of $\rho^*/2$ from the cellular boundary $A_p^* = -\rho^*/2$, this boundary is given by

$$\hat{b}^{3/2}(3+\hat{b})^{-2}\left[(3+\hat{b})(1-\hat{b})+8Pk\right]^2 = \alpha^{1/2}/k\,, \quad \alpha = 4{A_\Theta^*}^4/\rho^*\,. \tag{54}$$

In the limit $k \to \infty$, it is clear that that are two solutions of Eq. (54) given by $\hat{b} = 0$ (*i.e.*, $A_p^* = -\rho^*/2$) and $\hat{b} \sim -1 + 2(1+2Pk)^{1/2}$ (*i.e.*, $A_p^*/\rho^* \sim -(1+2Pk)^{1/2}$. Thus, the pulsating boundary is clearly multi-valued, as in the inviscid case (Fig. 3), with one branch approaching the cellular boundary and the other branch approaching the pulsating boundary for $A_\Theta = 0$ (Fig. 2) in the limit of large $k$. More generally, Eq. (54) may be rewritten as a cubic equation for the inverse relation $k(\hat{b})$ as

$$64P^2k^3 + 16(3+\hat{b})(1-\hat{b})Pk^2 + (3+\hat{b})^2(1-\hat{b})^2k - \alpha^{1/2}(3+\hat{b})^2\hat{b}^{-3/2} = 0\,, \tag{55}$$

which is clearly seen to collapse to the previous inviscid result [7] in the limit $P \to 0$. For arbitrary $P$, typical plots of $k(\hat{b})$ are shown in Figs. 4a–d, which, when rotated -90° so that the $k$-axis is horizontal, is readily interpreted in the context of Figs. 1 – 3, where the lines $A_p^* = -\rho^*/2$ and $A_p^* = -\rho^*$ correspond to $\hat{b} = 0$ and $\hat{b} = 1$, respectively. It is clear that these curves asymptote to the lines $\hat{b} = 0$ and $\hat{b} = -1 + 2(1+2Pk)^{1/2}$ as $k \to \infty$, where the latter corresponds to the viscous pulsating boundary in the limit $A_\Theta^* \to 0$. They cross the line $\hat{b} = 1$, which corresponds to the inviscid pulsating boundary in the above limit, at $k^3 = \alpha^{1/2}/4P^2$. The fact that the pulsating boundary becomes C-shaped (in the rotated frame of reference) for $A_\Theta^* > 0$ implies that steady, planar burning is intrinsically unstable for sufficiently small wavenumbers. In addition, since the portion within the C-shaped curve is the stable region, any crossing of the C-shaped boundary from the stable to the unstable region corresponds to the onset of a pulsating instability. As $A_\Theta^*$ increases, the turning point of the C-shaped pulsating boundary shifts to larger values of $k$. On the other hand, as $A_\Theta^*$ becomes small, the turning point shifts to small values of $k$ such that

this point eventually leaves the O(1) wavenumber region for which Eq. (54) are valid. Indeed, it turns out that the transition to separated pulsating and cellular branches occurs as $A_\Theta$ decreases through $O(\epsilon^{1/2})$ values for intermediate $O(\epsilon^{1/2})$ wavenumbers [7]. Thus, as $A_\Theta^*$ becomes small, the original pulsating and cellular boundaries are recovered in the O(1) wavenumber regime, but as $A_\Theta^*$ becomes large, the original cellular boundary lies within the unstable region for O(1) wavenumbers and the basic solution becomes intrinsically unstable to oscillatory disturbances.

## Composite Neutral Stability Boundary

A composite asymptotic solution for the neutral stability boundary in the regime $A_\Theta \sim O(\epsilon^{1/4})$ is thus obtained by matching the cellular and pulsating boundaries in the far outer wavenumber regime, where the former is given by Eq. (36) and the latter by the second of Eqs. (38), with the appropriate solution branch of Eq. (54) in the O(1) wavenumber region. In particular, reverting back to the parameter $A_p^*$, we denote the two solution branches of Eq. (54), which correspond to the portions of Figure 4 that lie to the left and to the right of the turning-point minimum, by $A_p^{*(o,u)}(k)$ and $A_p^{*(o,l)}(k)$, where the superscript "o" denotes, as before, the outer, or O(1), wavenumber region and the superscripts "u" and "l" denote the upper and lower (rotate Figure 4 by -90°) portions of the double-valued pulsating boundary $A_p^*(k)$. Along the upper branch, $A_p^{*(o,u)} \to -\rho^*/2$ (*i.e.*, $\hat{b} \to 0$) as $k \to \infty$, which can be matched with Eq. (36) since $A_p^{*(f)} \to -\rho^*/2$ as $k_f \to 0$. Similarly, $A_p^{*(o,l)} \to -\rho^*(1+2Pk)^{1/2}$ (*i.e.*, $\hat{b} \to -1+2(1+2Pk)^{1/2}$) as $k \to \infty$, which clearly matches the viscous pulsating boundary given by the second of Eqs. (38) in the far outer wavenumber region. As a result, a leading-order composite stability boundary spanning both the outer and far outer wavenumber regions is given by

$$A_p^*(k) \sim \begin{cases} A_p^{*(o,u)}(k) - \dfrac{\rho^*}{2} + \dfrac{2\rho^*\mu^* P\left[1+\epsilon k(\rho^*\gamma + 2\mu^* P + 2\rho^* P)\right]}{4\mu^* P(1+\rho^* P\epsilon k) - (1-[1+4\mu^{*2}P^2\epsilon^2 k^2]^{1/2})(\rho^*\gamma + 2\mu^* P)} \\ A_p^{*(o,l)}(k)\,, \end{cases} \tag{56}$$

for $A_p^* \gtrless A_p^{*c}$, where $A_p^{*c}$ denotes the turning point calculated from Eq. (54) and the second term in the top expression has been expressed in terms of the outer wavenumber variable $k$.

The composite stability boundary is shown in Fig. 5. Based on the above construction, the lower branch of Eq. (56) is a pulsating boundary for all wavenumbers, whereas the upper branch transitions from a pulsating boundary for O(1) wavenumbers to a cellular boundary for

$O(\epsilon^{-1})$ wavenumbers. Indeed, from Eq. (45), the size of the upper region of oscillatory instability, which is bounded below by the upper branch of the pulsating stability boundary and above by the region of nonoscillatory instability beyond the outer cellular boundary $A_p^* \sim -\rho^*/2$ for $A_\Theta^* = 0$, shrinks to zero as $k$ becomes large on the O(1) wavenumber scale. In this regime, the lack of a stable region for sufficiently small wavenumbers thus implies an intrinsic instability to long-wave pulsating perturbations.

## Conclusion

The present work further extends our recent formal treatment of hydrodynamic instability in liquid-propellant combustion. The analysis is based on a generalized Landau/Levich model in which the dynamic motion of the liquid/gas interface, assumed to coincide with the combustion front, realistically possesses both a pressure and temperature sensitivity. In the present work, the fully viscous case was considered, thereby generalizing previous analyses in which either the viscosity of the fluid and/or the temperature sensitivity of the reaction rate was neglected. As in these preceding studies, the smallness of the gas-to-liquid density ratio was used to define a small parameter that allowed an asymptotic treatment of a rather complex dispersion relation. Specifically, it was again shown that in addition to the classical Landau, or cellular, stability boundary, there exists a pulsating hydrodynamic stability boundary as well. For sufficiently small values of the temperature-sensitivity parameter, there is a stable region between these two boundaries corresponding to a range of negative pressure sensitivities for which steady, planar burning is stable.

As the pressure sensitivity decreases in magnitude, the cellular stability threshold is crossed, leading to classical Landau instability. Surface tension, viscosity (both liquid and gas), and gravity are all stabilizing effects with respect to this type of instability. However, only gravity stabilizes small-wavenumber disturbances, and thus Landau instability becomes a long-wave instability in the reduced-gravity limit. Alternatively, as the pressure-sensitivity parameter increases in magnitude, the pulsating boundary is crossed, and liquid-propellant combustion becomes unstable to oscillatory perturbations. This type of hydrodynamic instability is more sensitive to the stabilizing effects of (liquid) viscosity than is the cellular boundary, but the stabilizing influence of viscosity does not extend to small wavenumber disturbances, and gravity turns out not to have a significant effect on

this type of hydrodynamic instability. Consequently, for sufficiently large values of the temperature-sensitivity parameter, the pulsating boundary develops a turning point and becomes C-shaped. In this parameter regime, corresponding to ratios of the temperature-to-pressure sensitivities of the order of 200 – 1000, steady, planar combustion is intrinsically unstable to nonsteady long-wave perturbations. In that case, the pulsating form of hydrodynamic instability is predicted to dominate, leading to large unsteady cells along the burning liquid/gas interface.

## Acknowledgment

This work was supported by the United States Department of Energy under the contract DE-AC04-94AL85000 and by the NASA Microgravity Science Research Program under the contract C-32031-E.

## Nomenclature

| | |
|---|---|
| $A$ | burning rate |
| $A_p, A_\Theta$ | pressure-, temperature-sensitivity coefficients |
| $b_i$ | coefficients in perturbation solution ($i = 1, 2, \ldots, 10$) |
| $\mathbf{e}$ | rate-of-strain tensor |
| $Fr$ | Froude number |
| $g$ | inverse Froude number (gravitational acceleration) |
| $k$ | perturbation wavenumber |
| $\hat{\mathbf{n}}_s$ | unit normal |
| $p$ | pressure |
| $P$, $Pr$ | Prandtl number |
| $q$ | quantity defined below Eq. (26) |
| $r$ | quantity defined below Eq. (26) |
| $t$ | time variable |
| $\mathbf{u}$ | perturbation velocity vector |
| $\mathbf{v}$ | velocity vector |
| $(x, y, z)$ | moving coordinate system |
| $\gamma$ | surface-tension coefficient |
| $\epsilon$ | small bookkeeping parameter |
| $\zeta$ | perturbation pressure |
| $\lambda$ | gas-to-liquid thermal diffusivity ratio |
| $\mu$ | gas-to-liquid viscosity ratio |
| $\rho$ | gas-to-liquid density ratio |
| $\phi_s$ | perturbation in location of gas/liquid interface |
| $\Phi_s$ | location of gas/liquid interface |
| $\omega$ | complex perturbation frequency |

Subscripts, Superscripts:

| | |
|---|---|
| $i$ | inner wavenumber regime or integer variable |
| $f$ | far outer wavenumber regime |
| $l$ | liquid |
| $g$ | gas |
| $o$ | outer wavenumber regime |
| $*$ | scaled quantity |

## References


[1] Landau, L. D., "On the Theory of Slow Combustion," *Acta Physicochimica URSS*, Vol.19, 1944, pp. 77–85 and *Zh. Eksp. i Teor. Fiz.*, Vol. 14, 1944, p. 240.

[2] Levich, V. G., "On the Stability of the Flame Front When a Liquid is Burning Slowly," *Dokl. Akad. Nauk SSSR*, Vol. 109, 1956, pp. 975–978.

[3] De Luca, L., "Theory of Nonsteady Burning and Combustion Stability of Solid Propellants by Flame Models," *Nonsteady Burning and Combustion Stability of Solid Propellants*, edited by L. De Luca, E. W. Price and M. Summerfield, Vol. 143, Progress in Astronautics and Aeronautics, AIAA, Washington DC, 1992, pp. 519–600.

[4] Novozhilov, B. V., "Theory of Nonsteady Burning and Combustion Stability of Solid Propellants by the Zeldovich-Novozhilov Method," *Nonsteady Burning and Combustion Stability of Solid Propellants*, edited by L. De Luca, E. W. Price and M. Summerfield, Vol. 143, Progress in Astronautics and Aeronautics, AIAA, Washington DC, 1992, pp. 601–641.

[5] Margolis, S. B., "Hydrodynamic Instability in an Extended Landau/Levich Model of Liquid-Propellant Combustion at Normal and Reduced Gravity," *Combust. Flame*, Vol. 113, 1998, pp. 406–423.

[6] Margolis, S. B., "On Pulsating and Cellular Forms of Hydrodynamic Instability in Liquid-Propellant Combustion," *Twenty-Seventh Symposium (International) on Combustion*, The Combustion Institute, Pittsburgh, 1998, pp. 2375–2386.

[7] Margolis, S. B., "Pulsating Hydrodynamic Instability and Thermal Coupling in an Extended Landau/Levich Model of Liquid-Propellant Combustion — I. Inviscid Analysis," *Combust. Theory Modelling*, Vol. 4, 2000, to appear.

[8] Vosen, S. R., "The Burning Rate of Hydroxylammonium Nitrate Based Liquid Propellants," *Twenty-Second Symposium (International) on Combustion*, The Combustion Institute, Pittsburgh, 1989, pp. 1817–1825.

[9] Margolis, S. B., and Matkowsky, B. J., "Nonlinear Stability and Bifurcation in the Transition from Laminar to Turbulent Flame Propagation," *Combust. Sci. Tech.*, Vol. 34,, 1983, pp. 45–77.

[10] Armstrong, R. C., and Margolis, S. B., "Hydrodynamic and Reactive/Diffusive Instabilities in a Dynamic Model of Liquid Propellant Combustion," *Twenty-Second Symposium (International) on Combustion*, The Combustion Institute, Pittsburgh, 1989, pp. 1807–1815.

[11] Armstrong, R. C., and Margolis, S. B., "Hydrodynamic and Reactive/Diffusive Instabilities in a Dynamic Model of Liquid Propellant Combustion — II. Inviscid Fluid Motions," *Combust. Flame*, Vol. 77, 1989, pp. 123–138.

## Figure Captions

Fig. 1. Asymptotic representation of the cellular hydrodynamic neutral stability boundaries. The upper and lower sets of curves correspond to the normal and reduced-gravity regimes, respectively (curves drawn for the case $\epsilon = .04$, $\rho^* = 1.0$, $g = 6.0$, $g^* = 2.0$). The solid curves correspond to the inviscid limit ($P = 0$) with nonzero surface tension ($\gamma = 2.5$). The dash-dot curves correspond to nonzero surface tension ($\gamma = 2.5$) and liquid viscosity ($P = 1.0$), but zero gas-phase viscosity ($\mu^* P = 0$). The dash-dot-dot curves differ from the dash-dot curves by the addition of gas-phase viscosity ($\mu^* P = 1.0$), and are similar to the dash-dot-dot-dot curves, where the latter correspond to larger viscosities ($P = \mu^* P = 2.0$). The dash-dot-dot-dot-dot curves correspond to a viscous case ($P = \mu^* P = 1.0$), but with zero surface tension.

Fig. 2. Asymptotic representation of the pulsating hydrodynamic stability boundary for the viscous case ($P > 0$). The region between the pulsating and cellular boundaries (the latter are shown on an expanded scale in Fig. 1) is the stable region with respect to hydrodynamic instability.

Fig. 3. Composite pulsating/cellular hydrodynamic stability boundary for $A_\Theta \sim O(\epsilon^{1/4})$ in the limit of zero viscosity.

Figs. 4a–d. Pulsating hydrodynamic stability boundaries for $k \sim O(1)$ and $A_\Theta \sim O(\epsilon^{1/4})$ in the general viscous case. Figures are drawn for $\rho^* = 1$ and (a) $P = .001$; (b) $P = .01$; (c) $P = .1$; (d) $P = 1.0$.

Fig. 5. Composite pulsating/cellular hydrodynamic stability boundary for $A_\Theta \sim O(\epsilon^{1/4})$ in the general viscous case.

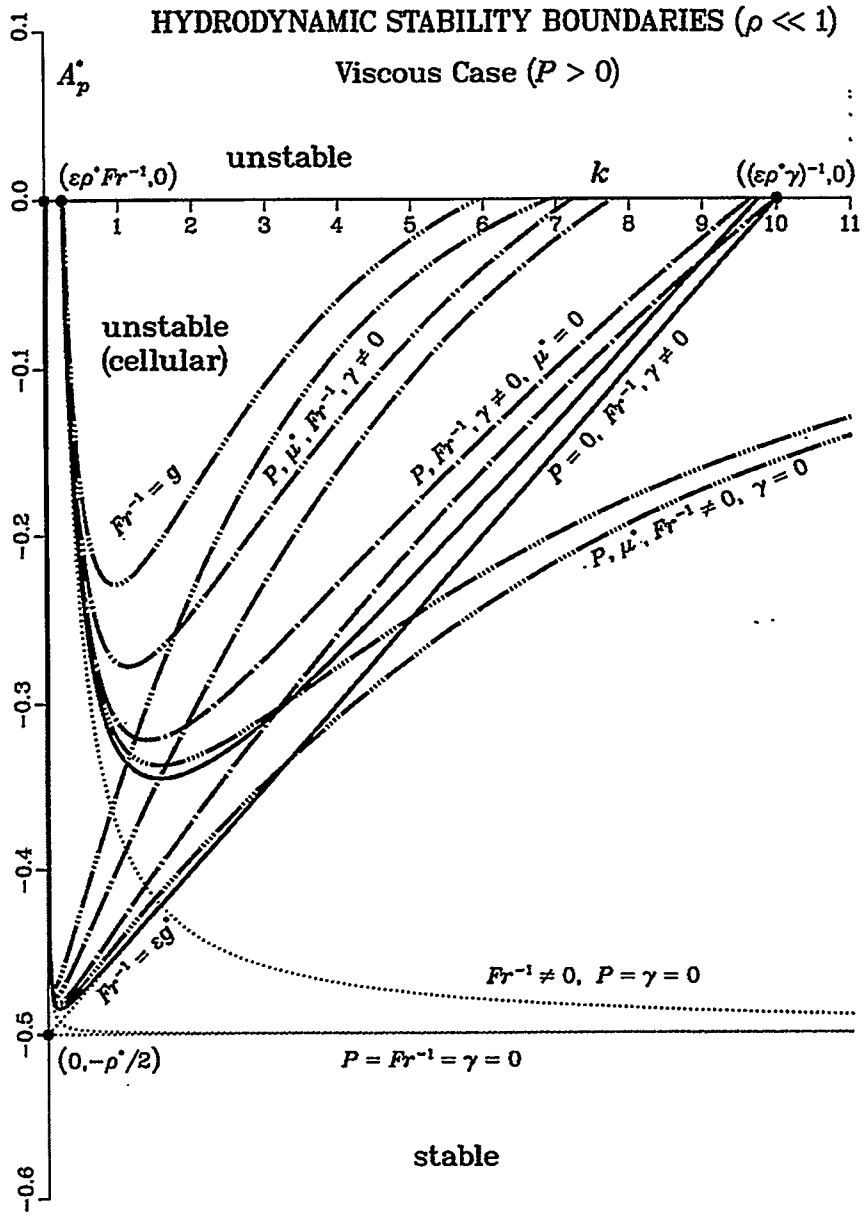
HYDRODYNAMIC STABILITY BOUNDARIES ($\rho \ll 1$)
Viscous Case ($P > 0$)
$A_p^*$
unstable
$k$
$(\varepsilon\rho^* Fr^{-1},0)$
$((\varepsilon\rho^*\gamma)^{-1},0)$
unstable (cellular)
$Fr^{-1} = g$
$P, \mu^*, Fr^{-1}, \gamma \neq 0$
$P, Fr^{-1}, \gamma \neq 0, \mu^* = 0$
$P = 0, Fr^{-1}, \gamma \neq 0$
$P, \mu^*, Fr^{-1} \neq 0, \gamma = 0$
$Fr^{-1} = \varepsilon g^*$
$Fr^{-1} \neq 0,\ P = \gamma = 0$
$(0,-\rho^*/2)$
$P = Fr^{-1} = \gamma = 0$
stable

Figure 1

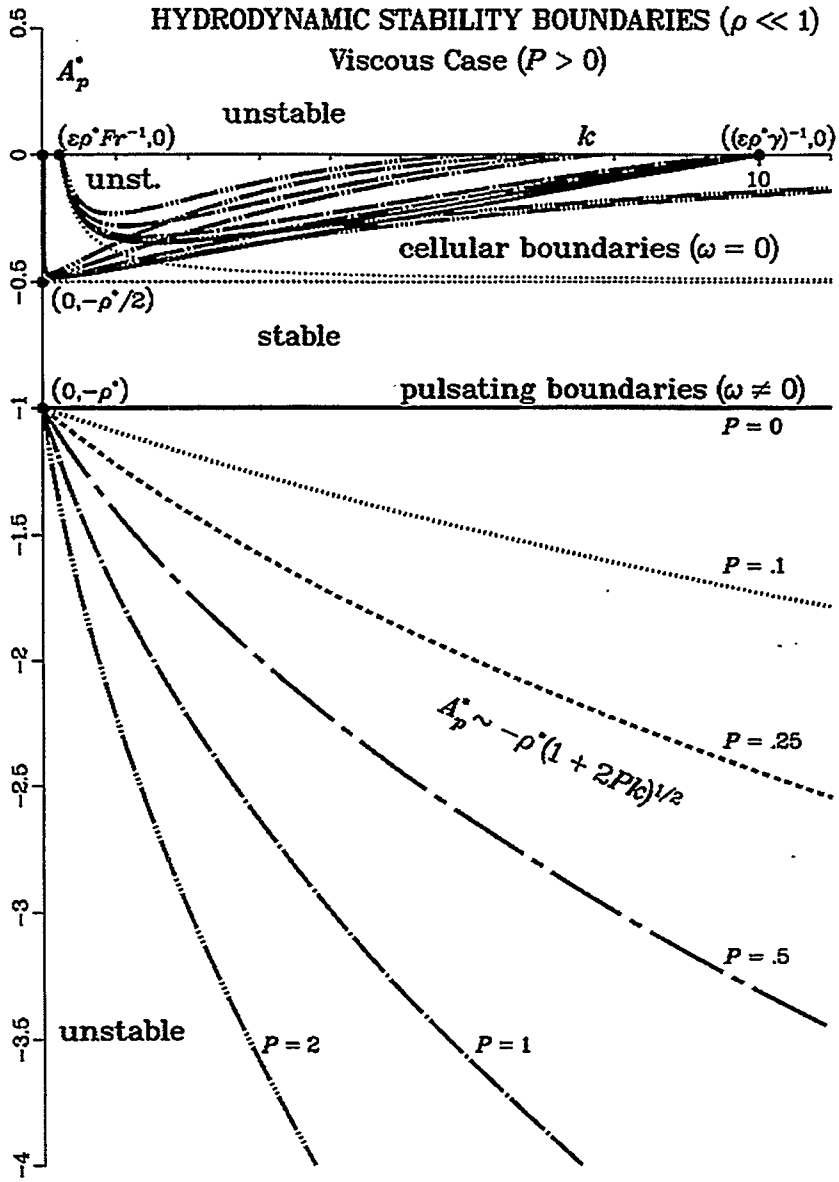
HYDRODYNAMIC STABILITY BOUNDARIES ($\rho \ll 1$)
Viscous Case ($P > 0$)
$A_p^*$
unstable
$(\varepsilon\rho^* Fr^{-1},0)$
$k_c$
$((\varepsilon\rho^*\gamma)^{-1},0)$
unst.
10
cellular boundaries ($\omega = 0$)
$(0,-\rho^*/2)$
stable
$(0,-\rho^*)$
pulsating boundaries ($\omega \neq 0$)
$P = 0$
$P = .1$
$P = .25$
$A_p^* \sim -\rho^*(1 + 2Pk)^{1/2}$
$P = .5$
unstable
$P = 2$
$P = 1$
0.5
0
−0.5
−1
−1.5
−2
−2.5
−3
−3.5
−4

Figure 2

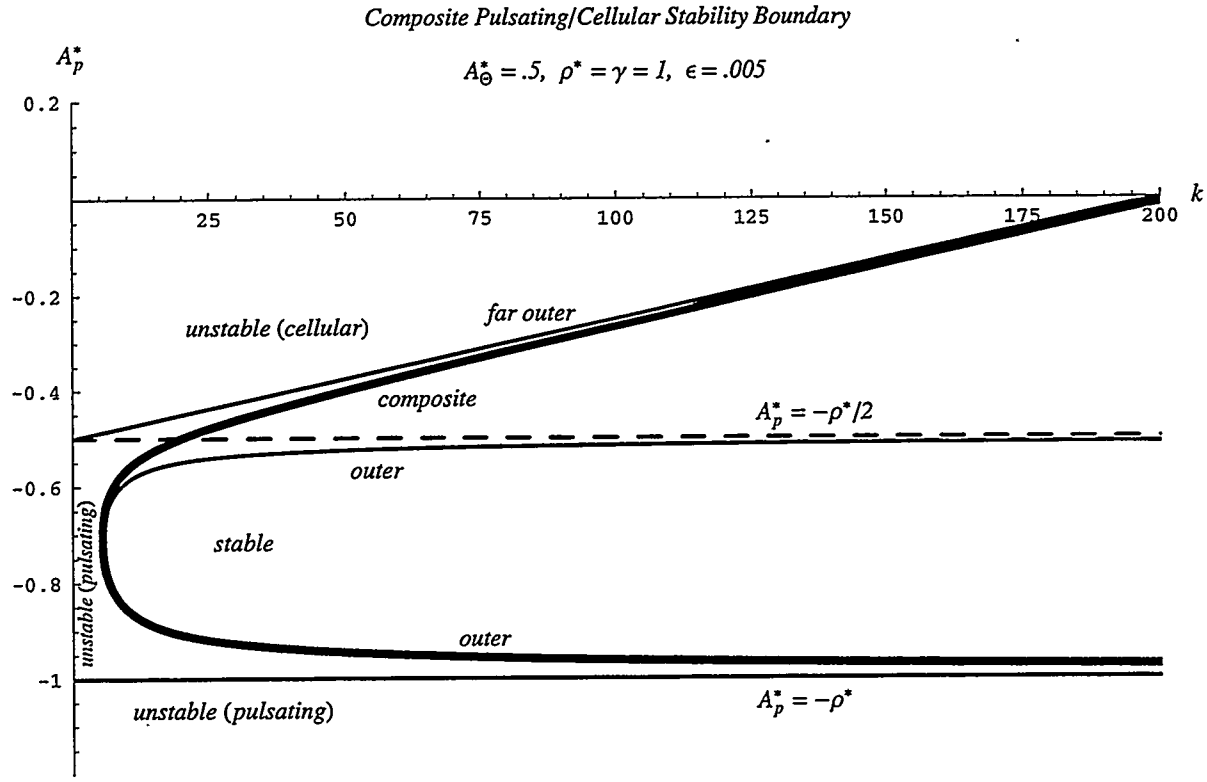
Composite Pulsating/Cellular Stability Boundary
$A_p^*$
$A_\Theta^* = .5,\ \rho^* = \gamma = 1,\ \epsilon = .005$
0.2
-0.2
-0.4
-0.6
-0.8
-1
25
50
75
100
125
150
175
200
$k$
unstable (cellular)
far outer
composite
$A_p^* = -\rho^*/2$
outer
stable
unstable (pulsating)
outer
unstable (pulsating)
$A_p^* = -\rho^*$

Figure 3

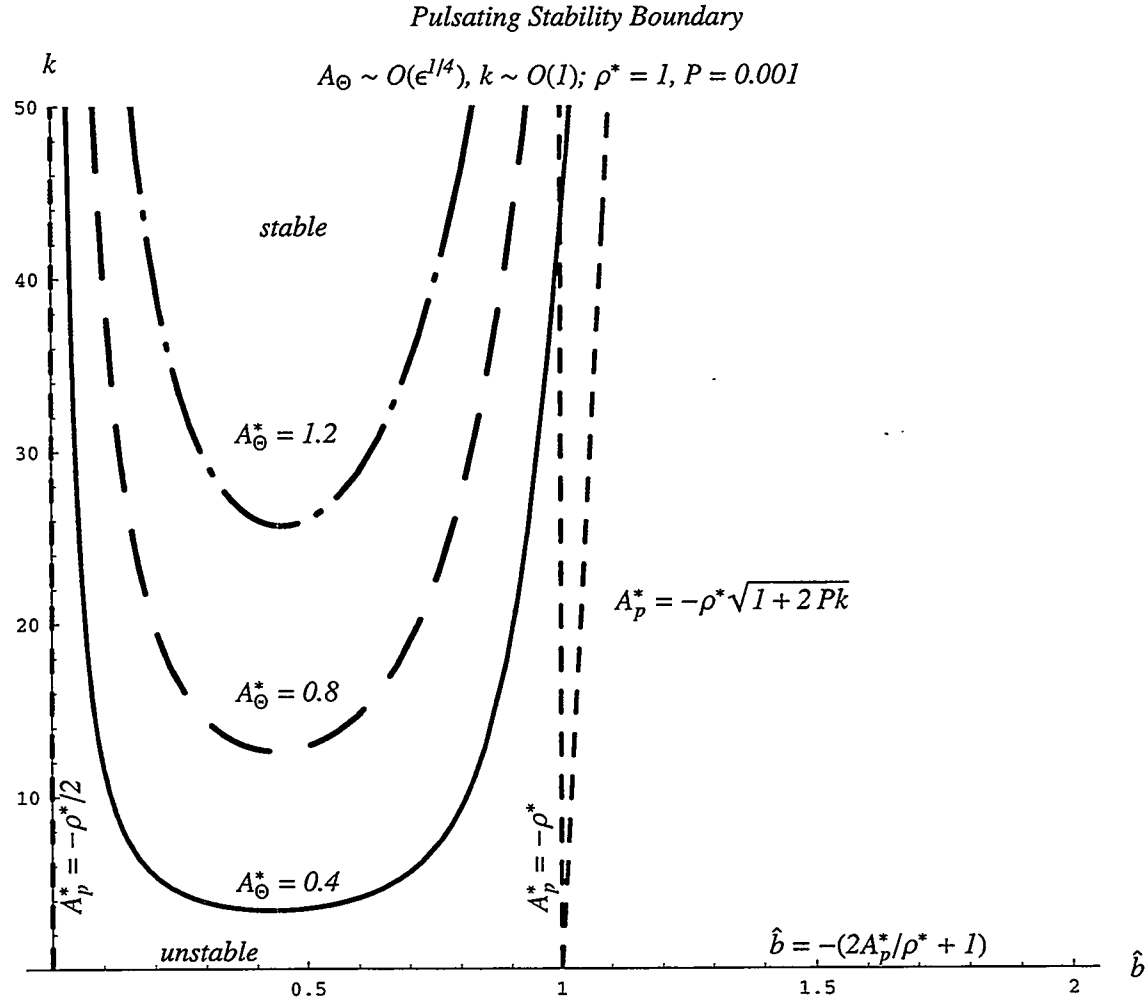
Pulsating Stability Boundary
$A_\Theta \sim O(\epsilon^{1/4})$, $k \sim O(1)$; $\rho^* = 1$, $P = 0.001$
k
50
40
30
20
10
stable
$A^*_\Theta = 1.2$
$A^*_\Theta = 0.8$
$A^*_\Theta = 0.4$
$A^*_p = -\rho^*\sqrt{1+2Pk}$
$A^*_p = -\rho^*/2$
$A^*_p = -\rho^*$
unstable
$\hat{b} = -(2A^*_p/\rho^* + 1)$
0.5
1
1.5
2
$\hat{b}$

Figure 4a

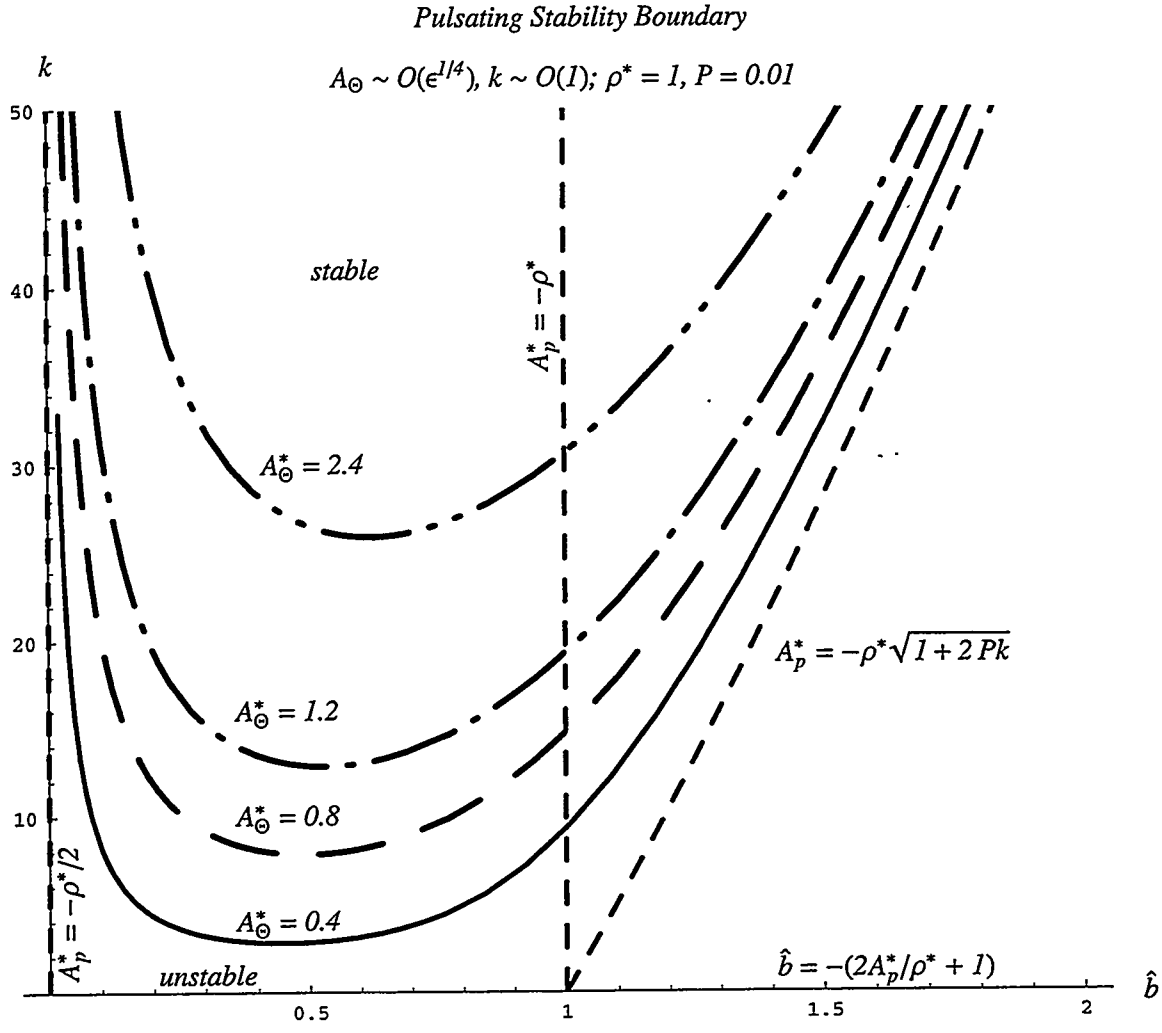
Pulsating Stability Boundary
$A_\Theta \sim O(\epsilon^{1/4})$, $k \sim O(1)$; $\rho^* = 1$, $P = 0.01$
k
50
40
30
20
10
stable
unstable
$A_p^* = -\rho^*$
$A_p^* = -\rho^*/2$
$A_\Theta^* = 2.4$
$A_\Theta^* = 1.2$
$A_\Theta^* = 0.8$
$A_\Theta^* = 0.4$
$A_p^* = -\rho^*\sqrt{1 + 2Pk}$
$\hat{b} = -(2A_p^*/\rho^* + 1)$
0.5
1
1.5
2
$\hat{b}$

Figure 4b

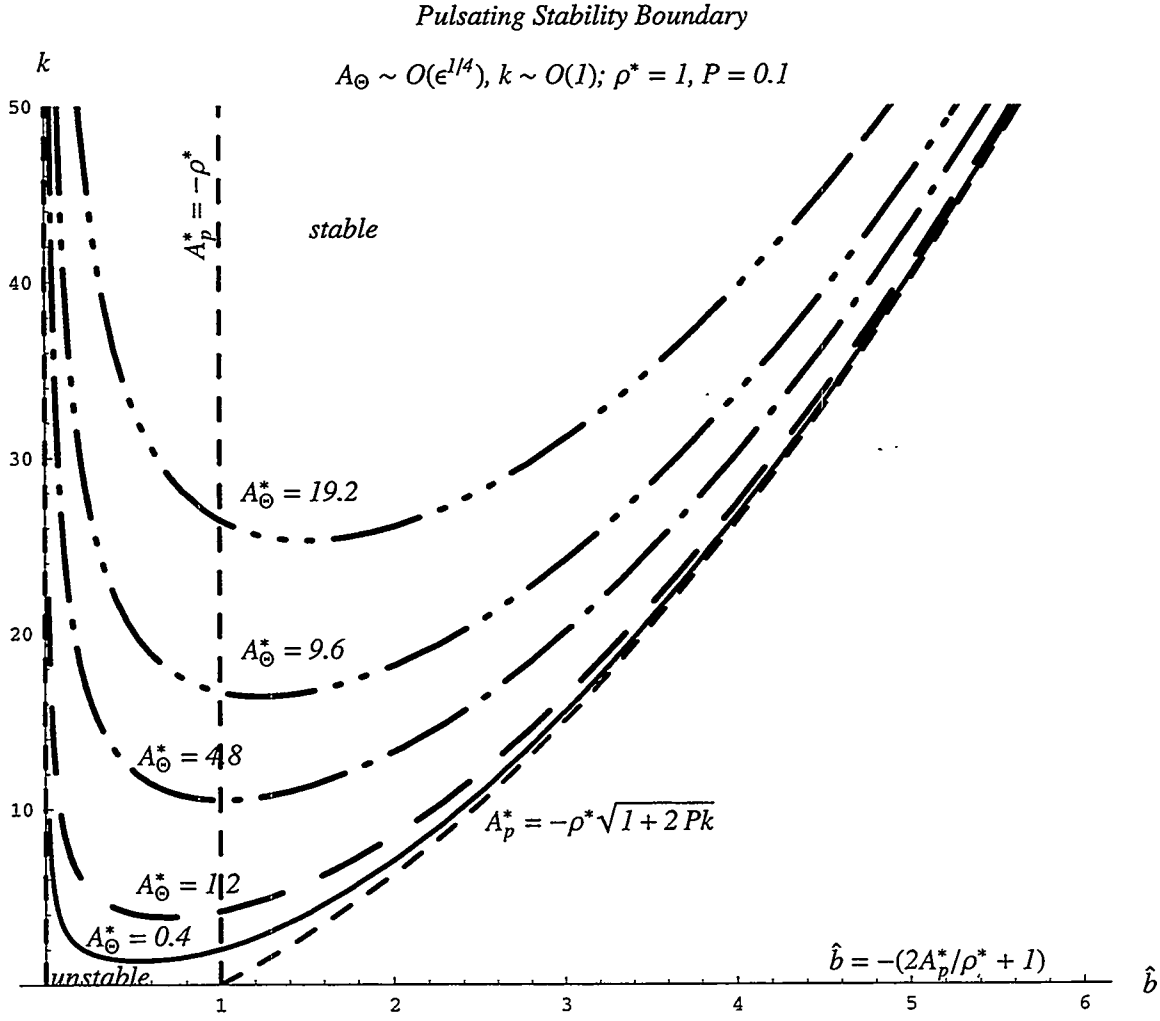
Pulsating Stability Boundary
$A_\odot \sim O(\epsilon^{1/4})$, $k \sim O(1)$; $\rho^* = 1$, $P = 0.1$
k
50
40
30
20
10
$A_p^* = -\rho^*$
stable
$A_\odot^* = 19.2$
$A_\odot^* = 9.6$
$A_\odot^* = 4.8$
$A_\odot^* = 1.2$
$A_\odot^* = 0.4$
unstable
$A_p^* = -\rho^* \sqrt{1 + 2Pk}$
$\hat{b} = -(2A_p^*/\rho^* + 1)$
$\hat{b}$
1
2
3
4
5
6

Figure 4c

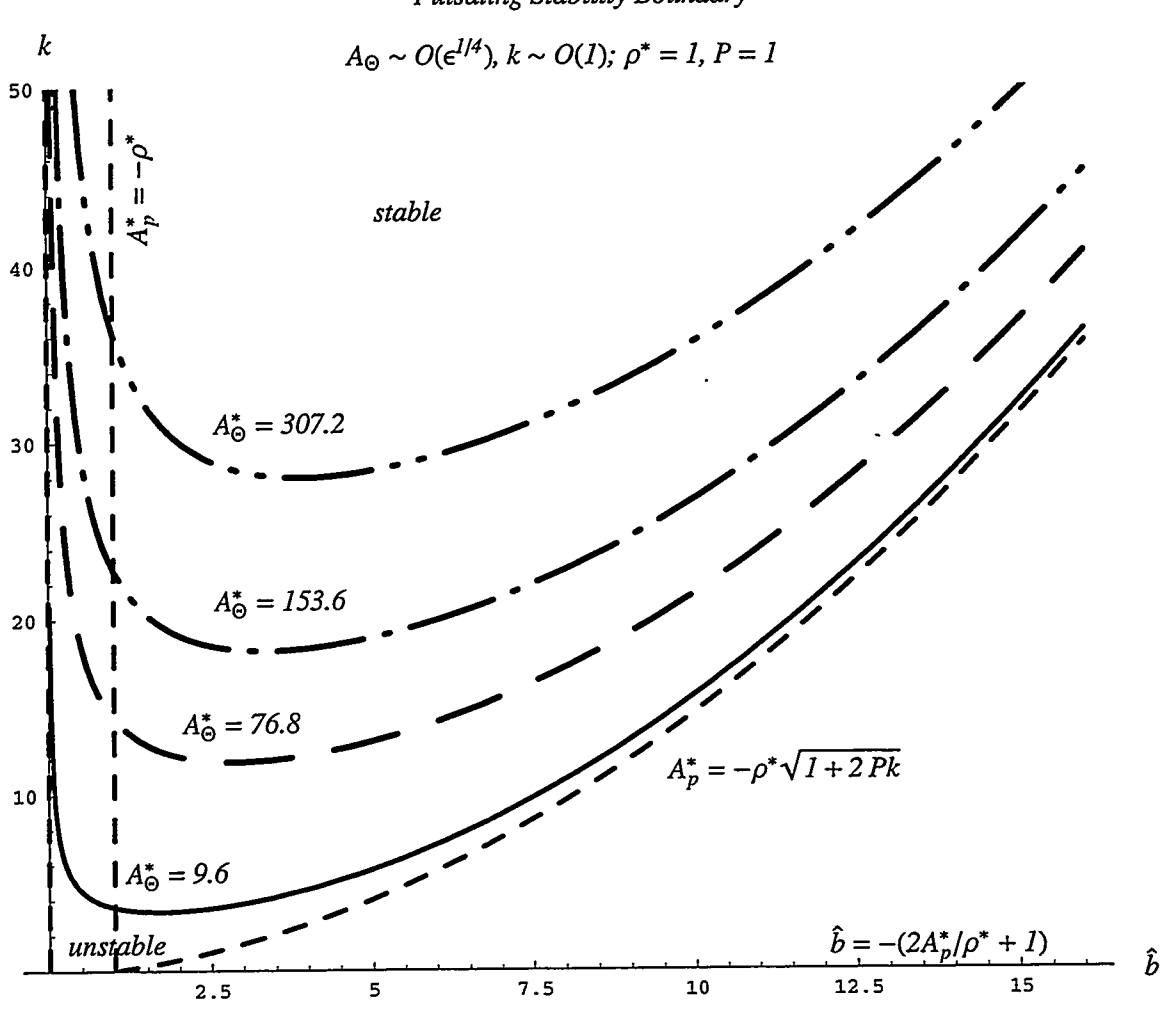
Pulsating Stability Boundary
$A_\Theta \sim O(\epsilon^{1/4})$, $k \sim O(1)$; $\rho^* = 1$, $P = 1$
k
50
40
30
20
10
$A_p^* = -\rho^*$
stable
$A_\Theta^* = 307.2$
$A_\Theta^* = 153.6$
$A_\Theta^* = 76.8$
$A_p^* = -\rho^*\sqrt{1+2Pk}$
$A_\Theta^* = 9.6$
unstable
$\hat{b} = -(2A_p^*/\rho^* + 1)$
$\hat{b}$
2.5
5
7.5
10
12.5
15

Figure 4d

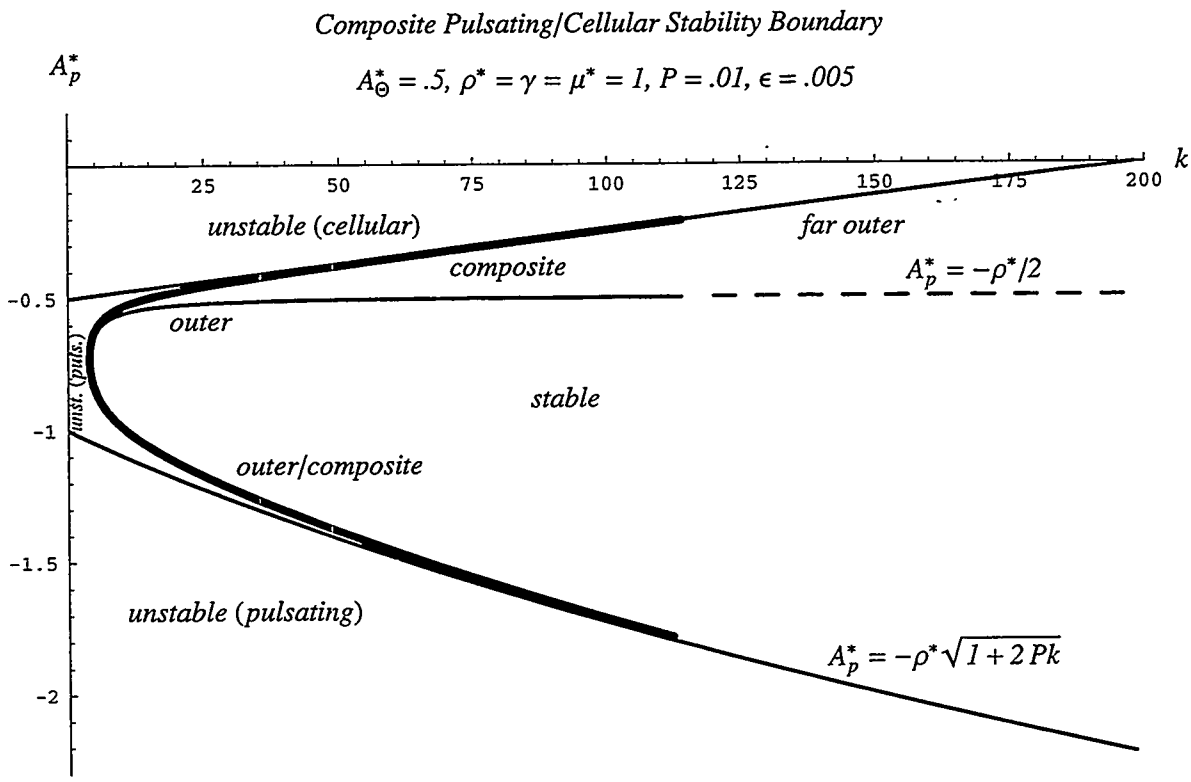
Composite Pulsating/Cellular Stability Boundary
$A_p^*$
$A_\Theta^* = .5,\ \rho^* = \gamma = \mu^* = 1,\ P = .01,\ \epsilon = .005$
k
25
50
75
100
125
150
175
200
-0.5
-1
-1.5
-2
unstable (cellular)
far outer
composite
$A_p^* = -\rho^*/2$
outer
inst. (puls.)
stable
outer/composite
unstable (pulsating)
$A_p^* = -\rho^*\sqrt{1+2Pk}$

Figure 5

UNLIMITED RELEASE

INITIAL DISTRIBUTION

Dr. John K. Bechtold
Department of Mathematics
New Jersey Institute of Technology
Newark, NJ 07102-1982

Dr. Mitat A. Birkan
Program Manager
Directorate of Aerospace and Engineering Sciences
Department of the Air Force
Bolling Air Force Base, DC 20332-6448

Prof. Michael Booty
Department of Mathematics
New Jersey Institute of Technology
Newark, NJ 07102-1982

Prof. John D. Buckmaster
Department of Aeronautical and Astronautical Engineering
University of Illinois
Urbana, IL 61801

Prof. Sebastien Candel
Ecole Central des Arts et Manufactures
Grande Voie de Vignes
92290 Chatenay-Malabry
FRANCE

Prof. J. F. Clarke
College of Aeronautics
Cranfield Institute of Technology
Cranfield-Bedford MK43 OAL
ENGLAND

Prof. Paul Clavin
Laboratoire Dynamique et Thermophysique des Fluides
Universite de Provence
Centre Saint Jerome
13397 Marseille Cedex 4
FRANCE

Prof. F. E. C. Culick
Jet Propulsion Center
California Institute of Technology
Pasadena, CA 91125

Prof. Martin Golubitsky
Department of Mathematics
University of Houston
University Park
Houston, TX 77004

Prof. Michael Gorman
Department of Physics
University of Houston
Houston, TX 77004

Dr. Daryl D. Holm
CNLS, MS 457
Los Alamos National Laboratory
Los Alamos, NM 87545

Prof. G. M. Homsy
Department of Chemical Engineering
Stanford University
Stanford, CA 94305

Dr. G. Joulin
Laboratoirie D'Energetique et de Detonique
Universite de Poitiers
Rue Guillaume VII
86034 Poitiers
FRANCE

Dr. Hans Kaper
Applied Mathematics Division
Argonne National Laboratory
9700 S. Cass Ave.
Argonne, IL 60439

Prof. A. K. Kapila
Department of Mathematical Sciences
Rensselaer Polytechnic Institute
Troy, NY 12128

Prof. D. R. Kassoy
Department of Mechanical Engineering
University of Colorado
Boulder, CO 80309

Prof. Joseph B. Keller
Department of Mathematics
Stanford University
Stanford, CA 94305

Prof. Barbara Keyfitz
Department of Mathematics
University of Houston
University Park
Houston, TX 77004

Prof. C. K. Law
Department of Mechanical and Aerospace Engineering
Engineering Quadrangle
Princeton University
Princeton, NJ 08544

Dr. Gary Leaf
Applied Mathematics Division
Argonne National Laboratory
9700 S. Cass Avenue
Argonne, IL 60439

Prof. Amable Liñán
Universidad Politecnica de Madrid
Escuela Tecnica Superior de Ingenieros Aeronauticos
Plaza del Cardenal Cisneros, 3
Madrid - 3
SPAIN

Prof. J. T. C. Liu
Division of Engineering, Box D
Brown University
Providence, RI 02912

Prof. Moshe Matalon
Department of Engineering Sciences and Applied Mathematics
Northwestern University
Evanston, IL 60208

Prof. Bernard J. Matkowsky
Department of Engineering Sciences and Applied Mathematics
Northwestern University
Evanston, IL 60208

Prof. A. C. McIntosh
Department of Fuel and Energy
University of Leeds
Leeds LS2 9JT
United Kingdom

Prof. D. O. Olagunju
Department of Mathematical Sciences
University of Delaware
Newark, DE 19716

Prof. R. E. O'Malley
Department of Applied Mathematics
University of Washington Seattle, WA 98195

Prof. Norbert Peters
Institute fur Allgemeine Mechanik
Technische Hochschule Aachen
Aachen
GERMANY

Prof. Victor Roytburd
Department of Mathematical Sciences
Rensselaer Polytechnic Institute
Troy, NY 12128

Prof. W. A. Sirignano
School of Engineering
University of California, Irvine
Irvine, CA 92717

Prof. L. Sirovich
Division of Applied Mathematics, Box F
Brown University
Providence, RI 02912

Prof. G. I. Sivashinsky
Department of Mathematics
Tel-Aviv University
Ramat-Aviv, Tel-Aviv 69978
ISRAEL

Prof. Mitchell D. Smooke
Department of Mechanical Engineering
Yale University
New Haven, CT 06520

Prof. D. Scott Stewart
Department of Theoretical and Applied Mechanics
University of Illinois
Urbana, IL 61801

Prof. C. H. Su
Division of Applied Mathematics, Box F
Brown University
Providence, RI 02912

Prof. Cesar Treviño
Departmento de Termica y Fluidos
Universidad Nacional Autonoma de Mexico
Facultad de Ingenieria
Patios No. 12, Jardines del Sur
MEXICO 23, D.F.

Prof. Vladimir Volpert
Department of Engineering Sciences and Applied Mathematics
Northwestern University
Evanston, IL 60208

Prof. Forman A. Williams
Department of Applied Mechanics and Engineering Sciences
University of California, San Diego
La Jolla, CA 92093

Prof. Vigor Yang
Department of Mechanical Engineering
Pennsylvania State University
University Park, PA 16802

Prof. Benn Zinn
Department of Aerospace Engineering
Georgia Institute of Technology
225 North Avenue, NW
Atlanta, GA 30332

C. K. Westbrook, LLNL, L-321

MS 1110 R. C. Allen, 1422
MS 0834 A. C. Ratzel, 9112
MS 0836 M. R. Baer, 9116
MS 0836 M. L. Hobbs, 9116
MS 0836 R. G. Schmitt, 9116

MS 9001 T. O. Hunter, 8000
MS 9405 R. E. Stoltz, 8008
MS 9004 M. E. John, 8100
MS 9054 W. J. McLean, 8300
MS 9163 W. Bauer, 8302
MS 9042 C. M. Hartwig, 8345
MS 9056 L. A. Rahn, 8351
MS 9051 W. T. Ashurst, 8351
MS 9051 A. R. Kerstein, 8351
MS 9052 D. R. Hardesty, 8361
MS 9055 R. Behrens, 8361
MS 9052 S. B. Margolis, 8361 (30)
MS 9053 R. W. Carling, 8362
MS 9021 Technical Communications Department, 8815, for DOE/OSTI
MS 9021 Technical Communications Department, 8815/Technical Library, MS 0899, 4916
MS 0899 Technical Library, 4916
MS 9018 Central Technical Files, 8940-2 (3)